Quantum Electronics **50** (5) 496–501 (2020)

NONLINEAR OPTICAL PHENOMENA https://doi.org/10.1070/QEL17185

Second-harmonic generation in zinc blende crystals under combined action of femtosecond optical and strong terahertz fields

S.B. Bodrov, A.I. Korytin, Yu.A. Sergeev, A.N. Stepanov

Abstract. **The influence of a short intense (with an electric field strength up to 250 kV cm^{-1}) terahertz (THz) pulse on the generation of second harmonic (SH) of Ti:sapphire laser radiation in crystals of zinc blende type (InAs and GaAs), characterised by nonzero bulk quadratic susceptibility, is investigated. It is experimentally shown for InAs(100) that, in the case of s-polarised first and second harmonics, an application of s-polarised THz field changes significantly the SH signal. The THz field-induced azimuthal dependence of the SH signal is in good agreement with the results of theoretical calculation within a phenomenological approach. The dependence of the SH signal on the delay time between the optical and THz pulses is investigated. This dependence for the GaAs crystal repeats the envelope of the THz pulse intensity, whereas in the case of InAs crystal there is a significant discrepancy, caused by the nonlinear dynamics of strong THz field in InAs.**

Keywords: *second harmonic, femtosecond laser pulses, THz field, zinc blende.*

1. Introduction

Second-harmonic generation (SHG) is one of the first demonstrated effects of nonlinear optics [1]. In zinc-blende-type GaAs and InAs crystals (point symmetry group $\bar{4}3m$) SHG is allowed (in the electric dipole approximation) in bulk [2]; however, since these crystals have a relatively narrow band gap, the second harmonic (SH) radiation in the visible and near-IR ranges undergoes strong absorption, as a result of which efficient SHG in their bulk is impossible. At the same time, these crystals are actively used to design metastructures, in particular, semiconductor lasers [3], waveguides [4], and various nanostructures [5, 6]. In view of the relatively small SH penetration depth into the crystal bulk, the SH characteristics are generally measured in backscattered geometry, where the surface contribution to the SHG may be comparable with that of the bulk source [7]; due to this, one can study surface effects.

One of the ways to develop the SHG method is to apply an external dc field to a sample under study. In this case an additional SH source is the cubic nonlinearity of the material, which makes it possible, in particular, to analyze the SHG in centrally symmetric media, where it is forbidden in bulk in the electric dipole approximation in view of the symmetry properties [8–10]. However, the use of dc fields for solving SHG problems has evident limitations. First, a system of electrodes must be designed to apply a dc field. The electric field distribution in the near-electrode regions may be fairly complicated. In addition, when studying crystalline samples, the position of deposited electrodes is rigidly fixed, for example, with respect to the crystallographic axes; this is an additional limitation on variation in parameters when carrying out experiments.

We propose to use intense ultrashort terahertz (THz) pulses to expand the potential of SHG method when studying various materials. A femtosecond laser is used as an optical radiation source, which provides sufficiently high intensities in material to implement efficient SHG. Due to the higher freedom (as compared with a dc field) in orienting the polarisation of electromagnetic THz field, one can increase the number of combinations of different polarisations (optical pumping–THz radiation–SH), characterising the nonlinear properties of the sample, and thus make experimental data more informative. In addition, the short (picosecond) duration of THz pulses makes it possible to investigate samples in strong electric fields (with a strength on the order 1 MV cm^{-1} or more), which cannot be done in the case of dc fields because of material breakdown. Such high strengths of THz pulse field (up to 100 MV cm^{-1}) were demonstrated previously [11]. Another important feature of the proposed approach is the possibility of studying SHG by changing the time delay between the optical and THz pulses. This means that the dynamics of the medium nonlinear response directly affecting SHG (phonon excitation, generation of free carriers, etc.) can be studied with a subpicosecond temporal resolution, determined by the THz pulse duration.

Note that the combining of optical pumping, second harmonic, and THz radiation was previously used in some works to diagnose THz fields [12, 13] and study the dynamics of molecular motion in liquids [14] or the lattice dynamics in inorganic ferroelectrics [15].

In this paper, we report the results of studying the influence of short-pulse THz radiation with an electric field strength up to 250 kV cm^{-1} on the generation of second optical harmonic of femtosecond laser radiation in crystals with a zinc-blende-type structure: InAs(100) and GaAs(100). Azimuthal dependences of the SH signal, caused by the components of both quadratic and cubic nonlinear susceptibility in crystals, are calculated within a phenomenological approach and confirmed experimentally. The dependence of SH signal on the delay time between optical and THz pulses is measured.

S.B. Bodrov, A.I. Korytin, Yu.A. Sergeev, A.N. Stepanov Institute of Applied Physics, Russian Academy of Sciences, ul. Ul'yanova 46, 603950 Nizhny Novgorod, Russia; e-mail: yas@ufp.appl.sci-nnov.ru

Received 11 November 2019; revision received 31 January 2020
Kvantovaya Elektronika **50** (5) 496–501 (2020)
Translated by Yu.P. Sin'kov

2. Calculation of azimuthal dependences

When studying crystalline samples, one of the main SHG characteristics is the azimuthal dependence of the SH signal on the sample rotation angle θ relative to the normal to the sample surface (Fig. 1). In this case the angle of incidence of light remains invariable, and the SH signal is determined by the dependence of the components of the induced nonlinear polarisation vector $P_{x,y,z}^{(2\omega)}$ on the angle θ in the laboratory coordinate system. Within the phenomenological approach, the nonlinear SH polarisation induced in a material by optical and THz fields $\boldsymbol{E}^{(\omega)}$ and $\boldsymbol{E}^{\mathrm{T}}$, respectively, can be presented in the electric dipole approximation [16] as

$$P_i^{(2\omega)} = \chi_{ijk}^{(2)} E_j^{(\omega)} E_k^{(\omega)} + \chi_{ijkl}^{(3)} E_j^{(\omega)} E_k^{(\omega)} E_l^{\mathrm{T}}, \tag{1}$$

where the subscripts i,j,k and l take values ξ,η and ζ, corresponding to the crystallographic axes. The first term on the right-hand side of (1) describes the contribution of quadratic nonlinearity and corresponds to the SHG induced by only the optical field. The second term, determined by cubic nonlinearity, corresponds to the SHG in the presence of additional (THz in our case) field. It follows from the symmetry of the zinc-blende-type lattice that the quadratic nonlinear susceptibility tensor $\chi_{ijk}^{(2)}$ in the crystallographic coordinate system has six identical nonzero components,

$$\chi_{\xi\eta\zeta}^{(2)} = \chi_{\xi\zeta\eta}^{(2)} = \chi_{\eta\zeta\xi}^{(2)} = \chi_{\eta\xi\zeta}^{(2)} = \chi_{\zeta\xi\eta}^{(2)} = \chi_{\zeta\eta\xi}^{(2)} \equiv \chi_0^{(2)}, \tag{2}$$

and the cubic nonlinear susceptibility tensor $\chi_{ijkl}^{(3)}$ has 21 nonzero components [2, pp 47, 53]:

$$\begin{aligned}
&\chi_{\xi\xi\xi\xi}^{(3)} = \chi_{\eta\eta\eta\eta}^{(3)} = \chi_{\zeta\zeta\zeta\zeta}^{(3)} \equiv \chi_1^{(3)},\\
&\chi_{\xi\xi\eta\eta}^{(3)} = \chi_{\eta\eta\xi\xi}^{(3)} = \chi_{\xi\xi\zeta\zeta}^{(3)} = \chi_{\zeta\zeta\xi\xi}^{(3)} = \chi_{\zeta\zeta\eta\eta}^{(3)} = \chi_{\eta\eta\zeta\zeta}^{(3)} \equiv \chi_2^{(3)},\\
&\chi_{\xi\eta\xi\eta}^{(3)} = \chi_{\eta\xi\eta\xi}^{(3)} = \chi_{\xi\zeta\xi\zeta}^{(3)} = \chi_{\zeta\xi\zeta\xi}^{(3)} = \chi_{\zeta\eta\zeta\eta}^{(3)} = \chi_{\eta\zeta\eta\zeta}^{(3)} \equiv \chi_2^{(3)},\\
&\chi_{\xi\eta\eta\xi}^{(3)} = \chi_{\eta\xi\xi\eta}^{(3)} = \chi_{\xi\zeta\zeta\xi}^{(3)} = \chi_{\zeta\xi\xi\zeta}^{(3)} = \chi_{\zeta\eta\eta\zeta}^{(3)} = \chi_{\eta\zeta\zeta\eta}^{(3)} \equiv \chi_3^{(3)}.
\end{aligned} \tag{3}$$

The result of recalculating the nonlinear polarisation in the laboratory coordinate system depends strongly on the crystal surface orientation. Having multiplied the tensors $\chi_{ijk}^{(2)}$ and $\chi_{ijkl}^{(3)}$ by the transition matrix from crystallographic to laboratory coordinate system, with allowance for the rotation by angle θ, we obtained analytical expressions for the nonlinear polarisation components $P_{x,y,z}^{(2\omega)}(\theta)$ for the (100) orientation of zinc-blende-type lattice. Below we report the corresponding expressions for only those nonlinear polarisation components that were experimentally investigated:

$$\text{s–s: } P_y^{(2\omega)} = 0, \tag{4}$$

$$\text{s–s–s: } P_y^{(2\omega)} = E_y^{\mathrm{T}} (E_y^{(\omega)})^2 [\chi_1^{(3)} - \Delta\chi + \Delta\chi\cos(4\theta)], \tag{5}$$

$$\text{p–s: } P_y^{(2\omega)} = 2\chi_0^{(2)} E_x^{(\omega)} E_z^{(\omega)} \cos(2\theta), \tag{6}$$

$$\begin{aligned}
\text{p–s–s: } P_y^{(2\omega)} &= 2\chi_0^{(2)} E_x^{(\omega)} E_z^{(\omega)} \cos(2\theta)\\
&+ E_y^{\mathrm{T}} \{\chi_1^{(3)} [(E_x^{(\omega)})^2 + (E_z^{(\omega)})^2]\\
&+ \Delta\chi (E_x^{(\omega)})^2 [1 - \cos(4\theta)]\}.
\end{aligned} \tag{7}$$

Abbreviated designations of the polarisations of fields involved in interaction (Fig. 1) are indicated on the left of the formulas. The electric field vector of p-polarised wave lies in the plane of incidence, whereas in the case of s-polarised wave the field vector is perpendicular to this plane. The first and last letters correspond to the polarisations of the first and second optical harmonics, respectively, while the letter in the middle (when there is one) corresponds to the THz field polarisation. In the s–s case, SHG is absent in the absence of THz field. An application of a THz field (the s–s–s case) gives rise to nonlinear polarisation, whose azimuthal dependence contains isotropic (independent of angle) component $\chi_1^{(3)} - \Delta\chi$, where $\Delta\chi = (\chi_1^{(3)} - 2\chi_2^{(3)} - \chi_3^{(3)})/4$, and an anisotropic component, proportional to $\Delta\chi\cos(4\theta)$. For the p–s case, as well as for the other (s–p and p–p) cases, SH generation in zinc-blende-type crystals with the (100) orientation is allowed in the electric dipole approximation. An application of THz field leads to additional contribution to the nonlinear polarisation, having both isotropic and anisotropic components. The value of this contribution depends linearly on the THz field strength and is determined by the nonlinear susceptibility tensor of higher (third) order.

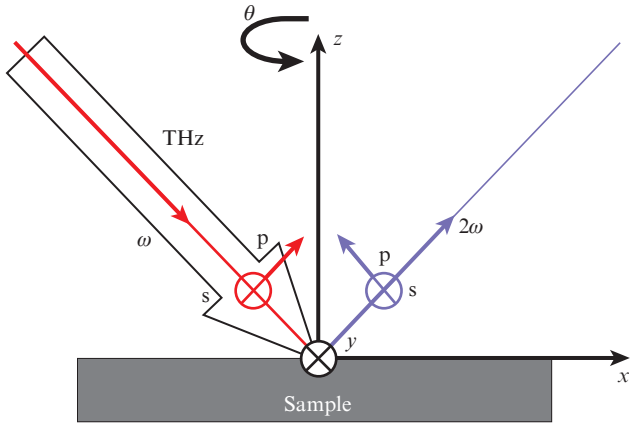

Figure 1. Geometry of the problem for calculating the azimuthal dependence.

3. Schematic of the experiment

The experimental setup for studying the SHG in semiconductor samples is shown in Fig. 2. The light source was a Ti:sapphire laser (Spitfire, Spectra-Physics), generating femtosecond pulses with a centre wavelength of 795 nm, an energy of 0.4 mJ, a pulse duration of 70 fs, and a repetition rate of 600 Hz. Most of the laser beam energy was used to generate THz pulses by the method of tilted intensity front in a nonlinear $LiNbO_3$ crystal [17]. The generated THz radiation was collected and focused tightly on the sample using a system of parabolic mirrors PM1, PM2, and PM3. The first two mirrors, PM1 and PM2, with effective focal lengths of 2.5 and 19 cm, respectively, were arranged confocally; they served to increase the THz beam transverse size. The third mirror, PM3, with an effective focal length of 5 cm and a diameter of 5 cm, focused THz pulses on the sample. The maximum THz field strength at the focal point was 250 kV cm^{-1}. The trans-

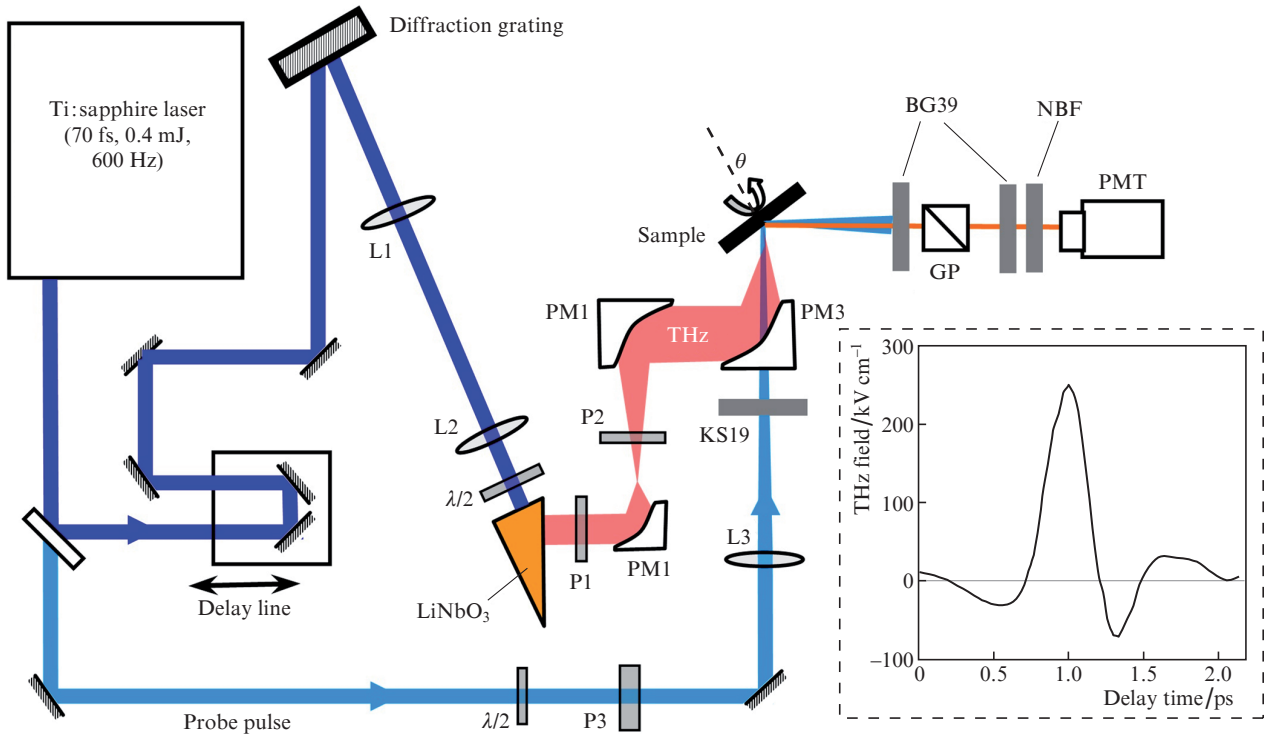

Figure 2. Schematic of the experimental setup: (L1, L2, L3) lenses; (PM1, PM2, PM3) parabolic mirrors; (GP) Glan prism; (KS19, BG39) optical filters; (NBF) narrowband filter (400 ± 40 nm); (P1, P2) THz polarisers; (P3) optical polariser; (PMT) photomultiplier tube. The inset shows the THz-field temporal profile.

verse size of the THz beam on the sample was about 500 μm at the half maximum of field amplitude. Two thin-film THz polarisers, P1 and P2 (Tydex), were used to change the THz field amplitude and polarisation.

A smaller (in energy) part of laser radiation (probe pulse) was used for SHG. The pulse energy and polarisation were varied using a $\lambda/2$ plate and an optical polariser. The probe optical beam was focused by lens L3 on the sample and aligned (after passing through a hole in mirror PM3) with the THz beam. A filter was installed before PM3 to cut off the spurious frequency-doubled radiation from the optical channel. The sample was fixed on a translation stage (rotating relative to the normal to the sample surface) and oriented at an angle of 45° with respect to the incident optical and THz beams. The SH signal was detected using a Hamamatsu R4220 photoelectron multiplier, with filters (cutting off foreign radiation) and a Glan prism at its input. A relative time delay between the optical probe pulse and THz pulse was implemented using a motorised delay line.

4. Experimental results and discussion

The SHG experiments were performed on samples of undoped InAs(100) and lightly doped GaAs(100) with a conductivity of 1 kΩ cm. The dependences of the SH signal on the energy of optical and THz pulses and the sample rotation angle θ at different relationships between the polarisations of the THz field and the first and second harmonics of light were investigated. We also analysed how a change in the delay between the THz and optical pulses affects the time dependence of the SH signal.

As was noted above, in view of the absence of central symmetry in the crystals studied, the SH is efficiently generated in the sample bulk for most relationships between the polarisations of the first and second harmonics. The influence of the THz field turned out to be insignificant for these combinations of polarisations and SH radiation. Figure 3 shows an angular dependence of the SH signal from an InAs crystal for the p–s case (the THz field was absent). Four maxima in the

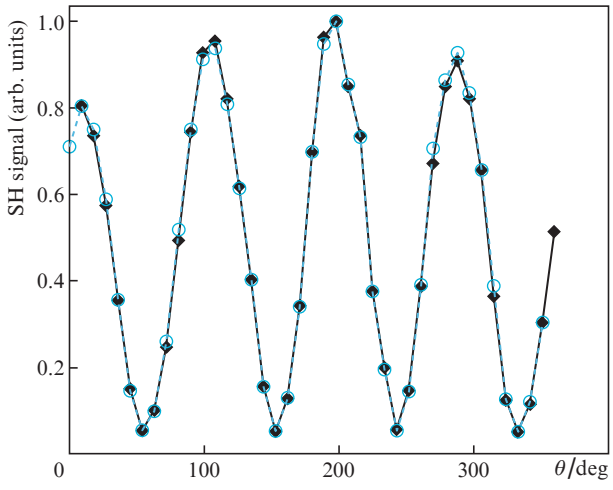

Figure 3. (Colour online) Azimuthal dependences of the SH signal generated in an InAs(100) crystal: the p–s (blue circles) and s–s–s (black rhombs) polarisation combinations.

angular dependence, which were previously experimentally observed in [8], are described well within the phenomenological model taking into account the crystal symmetry (see formula (7) and [8]). An application of s-polarised THz field (the p–s–s case in our designations) changes only slightly the SH signal.

As follows from the phenomenological theory for a crystal with the (100) orientation and zinc blende-type lattice, SHG should be absent for the s–s combination of polarisations of the first and second harmonics [see formula (4)]. However, an experimental study of this combination revealed a nonzero second-harmonic signal $S_{bg}(\theta)$, which depended on the azimuthal angle θ. This background (spurious) signal is most likely due to the error in orientating the sample crystallographic axes. Nevertheless, an application of s-polarised THz field (s–s–s combination) led to a significant increase and change in the azimuthal dependence. The thus obtained dependence $S(\theta)$ contained both the background signal $S_{bg}(\theta)$ and the THz-field induced informative signal $S_{THz}(\theta)$. To select the signal $S_{THz}(\theta)$, it was assumed that the phase of the sources of background and THz signals are shifted relative to each other by some constant value φ, which is independent of the azimuthal angle θ. Then, in the absence and in the presence of THz field, the SH signals from the sample surface can be presented, respectively, as $|A_{bg}(\theta)|^2$ and $|A_{bg}(\theta) + A_{THz}(\theta)\exp(i\varphi)|^2$, where $A_{bg}(\theta)$ is the background source amplitude and $A_{THz}(\theta)$ is the amplitude of the THz-field induced source (both amplitudes are considered to be real). Under the assumption that the dependence $A_{THz}(\theta)$ is described by (5), we compared the function $|A_{bg}(\theta) + A_{THz}(\theta)\exp(i\varphi)|^2$ with the experimental dependence $S(\theta)$, taking into account that $|A_{bg}(\theta)|^2 \propto S_{bg}(\theta)$. As a result, we found the unknown value φ and selected the informative signal $S_{THz}(\theta) \propto |A_{THz}(\theta)|^2$, which is shown in Fig. 4. It can be seen that the azimuthal dependence $S_{THz}(\theta)$ obtained from experimental data is described adequately by the function $(P_y^{(2\omega)}(\theta))^2$, where $P_y^{(2\omega)}(\theta)$ is determined by theoretical formula (5).

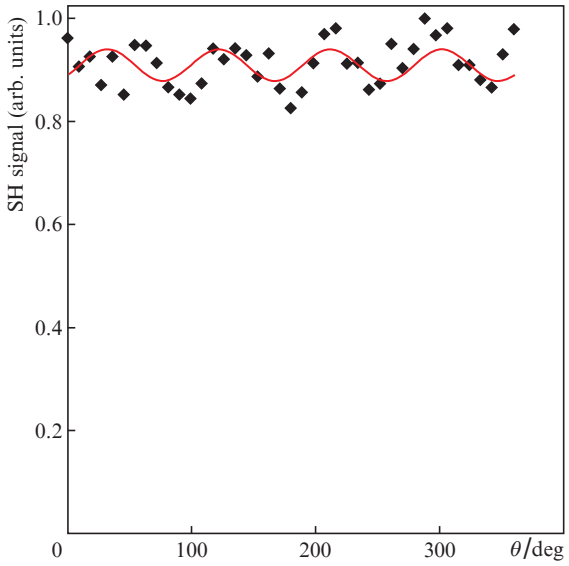

Figure 4. Azimuthal dependence of the SH signal induced by THz field in an InAs(100) crystal for the s–s–s polarisation combination (rhombs). The solid curve is an approximation of experimental data by the dependence of squared modulus of expression (5).

Figure 5 shows a dependence of the SH signal from InAs crystal on the squared THz field amplitude for the s–s–s combination of polarisations (the azimuthal angle θ was chosen such as to make the background signal $S_{bg}(\theta)$ negligible). The measurements were performed at a delay between the optical and THz pulses corresponding to the maximum THz field E_{THz}. The approximation of experimental data turned out to be close to linear, which is in agreement with theory [$S(\theta) \propto (P_y^{(2\omega)})^2 \propto E_{THz}^2$].

The dependence of the SH signal on the squared laser pulse energy W_{opt}^2 is presented in Fig. 6. It can be seen that exper-

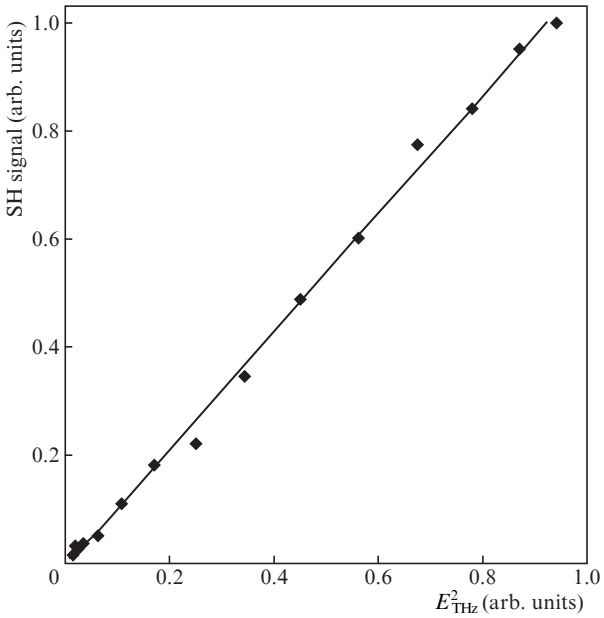

Figure 5. Dependence of the SH signal on the squared THz field, measured in an InAs(100) crystal for the s–s–s polarisation combination (rhombs). The solid line is a linear approximation of experimental data.

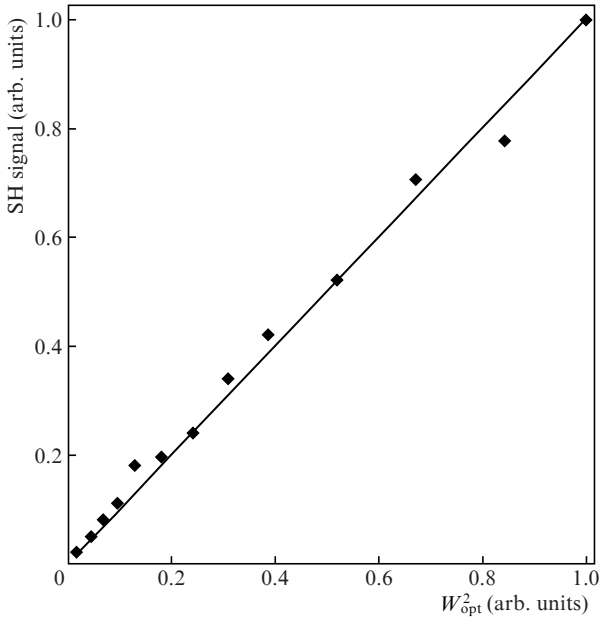

Figure 6. Dependence of the SH signal on the squared light pulse energy in an InAs(100) crystal for the s–s–s polarisation combination.

imental points fit well a straight line; i. e., the SHG under consideration is a nonlinear second-order process.

As was noted above, the joint use of femtosecond optical and short THz pulses allows one to investigate the SHG temporal dynamics by changing the time delay between the pulses. Figure 7 shows normalised time dependences of the SH signal for InAs(100) and GaAs(100) crystals in the case of the s–s–s polarisation combination, as well as the temporal shape of squared THz field strength, reconstructed from the experiments. For GaAs, as it was expected in correspondence with (1), the shape of SH signal mainly repeats the temporal profile of squared THz field (Fig. 7a). The difference of the measured SH signal from zero in the range of minima of squared THz field strength (at delay times of –0.25 and 0.2 ps) is explained by the finite optical pulse duration.

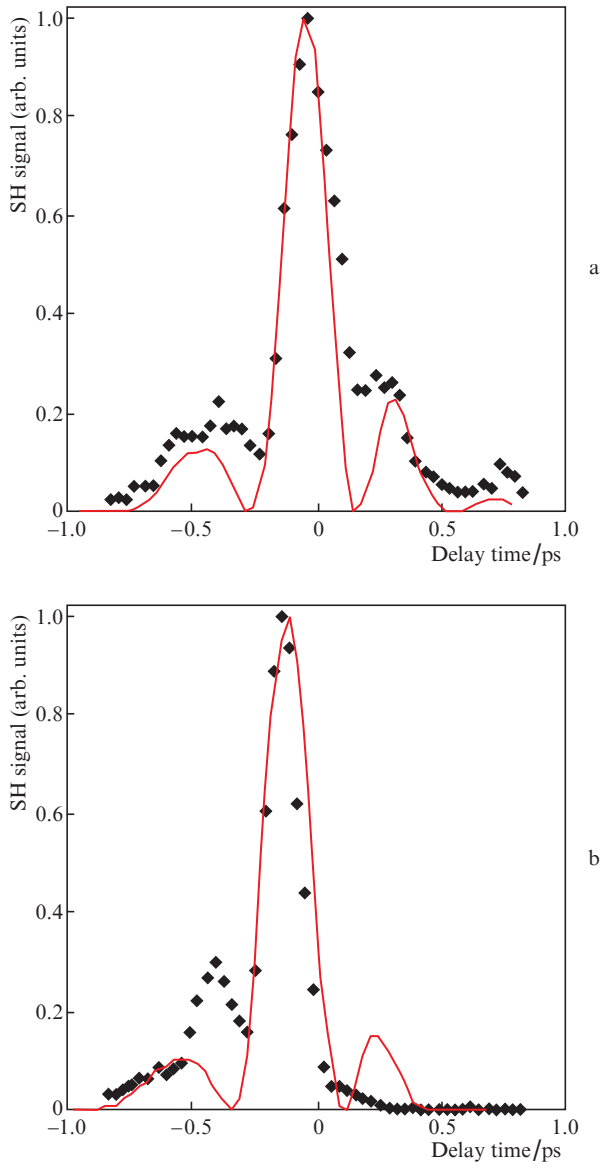

Figure 7. Experimental dependences of normalised SH signals (rhombs) on the delay time between the laser and THz pulses (femtosecond pulses arrive before THz pulses at the left side) for the (a) GaAs(100) and (b) InAs(100) crystals. The solid curves are temporal profiles of squared THz field amplitudes normalised to maximum.

The situation is radically different for the InAs crystal (Fig. 7b). In the vicinity of the left lateral maximum (at negative delays) the SH signal is much higher than the squared THz field amplitude normalised to maximum, whereas in the vicinity of the right lateral maximum (at positive delays) it is much lower. In our opinion, this fact can be explained by the distortion of the time dependence of THz pulse field in the InAs crystal, which is due to the influence of strong THz field on the electrodynamic properties of InAs. Indeed, even in the first lateral maximum the THz field strength exceeds 30 kV cm^{-1}. Such fields in InAs may cause impact ionisation and increase significantly the carrier concentration in the conduction band [18]. While the carrier concentration increases, the trailing part of the THz pulse becomes screened, and, correspondingly, the SH signal decreases, which manifests itself in the asymmetric temporal shape of SH signal. Gallium arsenide, which is characterised by a much wider band gap, does not exhibit any such anomalies in the SH temporal behaviour.

5. Conclusions

The influence of intense short THz pulses (with a field strength up to 250 kV cm^{-1}) on the generation of reflected SH of Ti:sapphire laser femtosecond radiation in zinc-blende-type InAs(100) and GaAs(100) crystals was investigated. The dependences of the SH signal on the azimuthal rotation angle of sample, THz field strength, and optical radiation energy were measured. It was shown that an s-polarised THz field changes significantly the SH signal when the first and second harmonics are also s-polarised; the reason is that the SH signal is zero in the absence of the THz field (within the dipole approximation). In this case, the measured azimuthal dependence of the SH signal is in good agreement with the theoretical phenomenological model. For other combinations of polarisations of the first and second harmonics the THz field barely affects the SH signal, which is due to a small contribution of the nonlinear polarisation induced by this field to the quadratic response of the medium (because of the nonzero quadratic susceptibility of the crystals studied). It was found that the dependence of the SH signal on the delay time between the optical and THz pulses in InAs crystals does not reproduce the theoretically predicted shape, corresponding to the time dependence of the squared THz field. In our opinion, this discrepancy is due to the nonlinear dynamics of the THz field (because of the influence of its high strength on the concentration and dynamics of carriers in InAs crystals).

Acknowledgements. This work was supported by the Russian Foundation for Basic Research and the government of Nizhny Novgorod region (Scientific Project No. 18-42-520070. The functioning of the laser system was partially maintained by the Ministry of Science and Higher Education of the Russian Federation within a government contract for the Institute of Applied Physics of RAS (Project No. 0035-2018-0023, Fundamental Research Programme 'Extreme Light Fields and Their Interaction with Matter' of the RAS Presidium).

References

1. Armstrong J.A., Bloembergen N., Ducuing J., Pershan P.S. *Phys. Rev.*, **127**, 1918 (1962).
2. Boyd R. *Nonlinear Optics* (New York: Academic Press, 2008).
3. Fedorova K.A., Sokolovskii G.S., Battle P.R., Livshits D.A., Rafailov E.U. *Opt. Lett.*, **40**, 835 (2015).

4. Rivoire K., Buckley S., Hatami F., Vučković J. *Appl. Phys. Lett.*, **98**, 263113 (2011).
5. Pecora E.F., Walsh G.F., Forestiere C., Handin A., Russo-Averchi E., Dalmau-Mallorqui A., Canales-Mundet I., Morral A.F., Dal Negro L. *Nanoscale*, **5**, 10163 (2013).
6. Sanatinia R., Swillo M., Anand S. *Nano Lett.*, **12**, 820 (2012).
7. Yamada C., Kimura T. *Phys. Rev. Lett.*, **70**, 2344 (1993).
8. Reid M., Cravetchi I.V., Fedosejevs R. *Phys. Rev. B*, **72**, 035201 (2005).
9. Aktsipetrov O.A., Baranova I.M., Evtyukhov K.N. *Nelineinaya optika kremniya i kremnievykh nanostruktur* (Nonlinear Optics of Silicon and Silicon Nanostructures) (Moscow: Fizmatlit, 2012).
10. Maker P.D., Terhune R.W. *Phys. Rev.*, **137**, 801 (1965).
11. Vicario C., Ovchinnikov A.V., Ashitkov S.I., Agranat M.B., Fortov V.E., Hauri C.P. *Opt. Lett.*, **39**, 6632 (2014).
12. Nahata A., Heinz T.F. *Opt. Lett.*, **23**, 67 (1998).
13. Chen J., Han P., Zhang X.-C. *Appl. Phys. Lett.*, **95**, 011118 (2009).
14. Cook D.J., Chen J.X., Morlino E.A., Hochstrasser R.M. *Chem. Phys. Lett.*, **309**, 221 (1999).
15. Grishunin K.A., Ilyin N.A., Sherstyuk N.E., Mishina E.D., Kimel A., Mukhortov V.M., Ovchinnikov A.V., Chefonov O.V., Agranat M.B. *Sci. Rep.*, **7**, 687 (2017).
16. Shen Y.R. *The Principles of Nonlinear Optics* (New York: Wiley, 1984; Moscow: Nauka, 1989).
17. Fulop J.A., Palfalvi L., Almasi G., Hebling J. *Opt. Express*, **18**, 12311 (2010).
18. Ho I.-C., Zhang X.-C. *Appl. Phys. Lett.*, **98**, 241908 (2011).